Strain-induced changes of the X-ray diffraction patterns of cross-linked poly(dimethylsiloxane): the texture hypothesis

Xiang Shi, Pierre-Antoine Albouy, Pascale Launois

Polymer 247 (2022) 124760

Strain-induced changes of the X-ray diffraction patterns of cross-linked Poly (dimethylsiloxane): The texture hypothesis

Xiang Shi, Pierre-Antoine Albouy *, Pascale Launois

Laboratoire de Physique des Solides, UMR CNRS 8502, Université Paris-Saclay, 91405, Orsay, France

ARTICLE INFO

Keywords:
Crystal structure
Orientation
X-ray diffraction

ABSTRACT

Poly(dimethylsiloxane) is a widely used silicone polymer that undergoes partial crystallization both as free oil and rubber when sufficiently cooled. However, a description of its crystalline structure surprisingly remains a totally open question. In particular X-ray diffraction fiber patterns of stretched silicone rubbers display impressive changes with strain and a recently proposed explanation involves a rich polymorphism. The present study develops the different idea that the X-ray pattern evolution merely reflects changes in the crystalline texture: a single crystalline phase is present with a structure virtually unaffected by strain while the axis of preferential orientation for the crystallites progressively changes. This enables a quantitative description of the X-ray fiber patterns, but the remaining fundamental structural issues are underlined.

1. Introduction

Poly(dimethylsiloxane) (PDMS) is the most widely used silicon-based organic polymer and it is an astonishing fact that the structure of its low-temperature crystalline phase still remains an open question. It forms oils of high thermal stability and adjustable viscosity when containing free chains with linear or branched structures, and it can be cross-linked to yield so-called silicone rubbers. These last are most frequently reinforced by the addition of divided silica as filler. PDMS readily crystallizes when cooled within a broad range of molecular weight, cross-link density and filler content [1–5]. The crystallization kinetics is usually maximum around 210K and the crystallinity can reach values above 50%. The melting temperature in the quiescent state is ca. 236K and the T_g is ca. 150K.

A first crystalline structure was proposed in 1962 by Damaschun, based on the analysis of X-ray diffraction fiber patterns of a highly-stretched piece of silicon rubber (extension ratio: 4, 35% Aerosil silica filler) [6]. Only sketches describing the experimental position of the intensity reinforcements for the three most intense inner diffraction rings are provided, probably due to experimental limitations. Diffraction layers perpendicular to the draw axis are tentatively drawn and the observation of a meridional reflection located on the second-order layer was interpreted as evidence for a two-fold screw axis (2_1) aligned along the stretching direction. Such a symmetry element points to a monoclinic structure and the author proposed a model where the unit cell contains a single polymer chain that adopts a rather relaxed twofold helical conformation with six monomers per turn. This implies the existence of three independent monomeric units which was contradicted by a subsequent NMR study by Schilling et al., in 1991 [7]. Indeed, they observed a single resonance for the ^{29}Si and ^{13}C nuclei that means that all monomers are equivalent within the unit cell. In 2000, one of us performed a new X-ray diffraction study based on low-extended PDMS rubber samples (draw ratio ca.2) [8]. The fiber patterns were found surprisingly different from Damaschun's report, although the reported d-spacings for the first three most intense reflections were similar. A reflection in meridional position was only observed on the fourth-order layer that pointed to four-fold 4_1 symmetry and hence to a tetragonal structure. This hypothesis was comforted by (i) the nice agreement between experimental and computed d-spacings for the ten first diffraction rings using a body-centered tetragonal unit cell (ii) the possibility to precisely account for the texture pattern with this assignment. The density for the crystalline phase was estimated by X-ray absorption measurements to ca. 1.16 g/cm^3 that corresponds to eight monomers per unit cell. The space group $I4_1$ was proposed where two chains are related by the centering condition and are running parallel to the c-axis: all monomers within the unit cell are equivalent in agreement with NMR data. This structure implies a highly extended four-fold helical chain conformation with four monomers per turn deemed possible by the high flexibility of the siloxane link. The atomic positions could not be refined with this structural model and this impossibility was attributed to some structural disorder. Based on the d-spacings similarities, the differences in the fiber patterns obtained at low and high draw ratios were explicitly attributed to a change in the crystallites orientation (texture) and not in their structure.

This problematic was recently revisited by M Tosaka at al. and their results are exposed in two publications. They first led a detailed study of the impact of the applied draw ratio on the fiber patterns [9]. They confirmed the existence of two generic patterns typical for low extension (up to ca. 2) and high extension (above ca. 3.5) and they evidenced for the first time the intermediate steps. Low-stretch patterns were attributed to a tetragonal crystalline modification ("β-form") and high stretch patterns to a monoclinic crystalline modification (α-form). As underlined above the two different crystal structures are associated to similar d-spacings and the authors were aware of this anomaly. In a second publication mainly based on the direct observation by low-temperature electron microscopy of tiny PDMS single-crystals directly grown on the TEM grid [10], the authors proposed a richer polymorphism with four possible crystalline modifications in the quiescent state. The evolution of the fiber patterns was explained by changes in the respective proportions of crystalline phases whose detailed structural description is out of the scope of the present work. One possible objection to this model is that the structural description proposed for each phase is derived from a restricted set of electronic diffraction data. Zhao et al. very recently used this four phases model to analyze diffraction patterns obtained during mechanical cycling measurements at low temperatures (−75 °C to −35 °C) and for various strain rates [11–13].

We decided to revisit this question in the frame of a broader study on the influence of pre-extension on the crystallization process in PDMS rubber [14]. In what follows an alternate model is proposed based on a progressive change in preferential orientation axis with increasing extension while keeping a virtually unchanged unique crystalline structure. We show how this may quantitatively account for both the diffraction line positions in the quiescent state and for the progressive fiber pattern evolution.

2. Experimental section

2.1. Materials

A precise determination of crystallographic parameters requires the growth of as large as possible crystallites and we used a PDMS oil to avoid size limitations by chemical cross-links (Gelest: DMS-V31: vinyl-terminated PDMS, M_w = 28000 g). PDMS rubbers necessary for the stretching experiments were prepared by cross-linking a vinyl-terminated oil (Gelest: DMS-V33; M_w = 43000 g) with tetrakis(dimethylsiloxy)silane as cross-linker (Gelest: SIT7278.0); the reaction was conducted at 80 °C in presence of the Speier catalyst. The silica filler was grown in situ closely following a sol-gel process described in the literature and known to be very efficient for reinforcement [15–17]. This efficiency could be related to the higher than expected value for the strain-amplification factor demonstrated by Shi [14] (the strain-amplification factor in filled elastomers is defined as the ratio of the actual strain experienced by the polymer matrix to the applied strain). The samples presently used contain 24phr silica and the strain amplification factor is estimated to ca. 1.9; they are obtained as ca. 0.7 mm thick foils with typical lateral dimensions 10 × 10cm^2. This peculiar filling method presents two specific advantages for the present study. First, draw-ratios necessary to follow the fiber pattern evolution are significantly diminished and samples are much easier to fix into the cryostat. A second and more significant advantage is better-defined fiber patterns at lower draw ratios compared to those from samples reinforced by addition of silica powder.

2.2. X-ray diffraction set-ups

A helium close-cycle cryocooler operated under vacuum and equipped with beryllium windows was used for all measurement; the cooling rate is limited to ca. 1.5 K/min by the apparatus cooling power. The cooler was mounted either on a MAR 345 detector for texture measurements (rotating anode generator; molybdenum target, wavelength: 0.0711 nm; multi-layer parallel optic) or on a homemade powder diffractometer for the crystallographic parameters determination (rotating anode generator; copper target, wavelength: 0.1542 nm; multi-layer parallel optic); the experimental resolution of this last set-up is $\delta q_{1/2}$ = 0.049 nm^{-1} and it is equipped with a position sensitive detector that offers the possibility to reconstruct complete powder patterns from a few acquisitions performed at fixed angular positions. Rubber samples used for fiber pattern acquisition are cut in bands ca. 2 mm wide and 10 mm long that are pre-stretched to a given draw-ratio at room temperature and clamped onto a copper substrate for proper thermalization. Cooling is thus performed at constant applied deformation similar to Tosaka's procedure. This must be distinguished from the dynamical experiments led by Zhao et al. [11–13].

3. Results and discussion

3.1. Unit cell parameters

DSC thermograms of PDMS quite often exhibit two melting peaks usually explained by melting/recrystallization processes that generate two populations of crystallites with different sizes [1,18]. In that case the lower temperature peak is attributed to the melting of less stable smaller and possibly partially disordered crystallites. That might be detrimental to a precise evaluation of crystallographic parameters that requires a homogeneous population of well-grown crystallites. Two cooling schemes have been thus tested: the sample is directly cooled down to 164K during process #1. For process #2 the sample is first cooled till some crystallization is detected, then progressively warmed up close but below complete melting. The remaining crystallites are assumed to act as seeds during the subsequent cooling sequence down to 164K. The two processes are compared by recording the evolution of the intensity of four intense diffraction lines during the final warming sequence (data acquisition with a position-sensitive detector at a fixed position; acquisition time: 10").

The evolution of the scattered intensity for the crystalline phase is plotted in Fig. 1-A: it clearly shows a first drop at ca. 224K after cooling process #1 that can be associated to the melting of a less-stable crystallite population. Final melting starts at ca. 240K and is achieved at 243K. No such well-defined pre-melting is observed after cooling process #2 and complete melting is observed at 245K. A sharp decrease ca. 10^{-3} in relative value in the line positions is similarly detected at 224K after cooling process #1 (see Fig. 1-B). It can be related to the melting of the less stable crystallite population, assuming they possess a slightly larger unit cell probably due to surface energy effects. A continuous increase is simply observed for cooling process #2 that reflects progressive thermal expansion. It suggests that one population of crystallites is essentially present after cooling process #2, and all data presented in what follows have been collected in these conditions.

Powder patterns were recorded at 153K and 223K up to a scattering vector ca. 43 nm^{-1}: see Fig. 2. The different lines display quite similar half-widths at half-intensity $\delta q_{1/2}$ after correction for resolution, ca. 510^{-2} nm^{-1}; it indicates well-grown and rather isotropic crystallites with a size L about 55 nm according to the Scherrer formula L ~$0.9\pi/\delta q_{1/2}$ [19].

The diffractogram present numerous doublets that are not all easy to resolve precisely. Experimental d-spacings collected in Table 1 only refer to diffraction lines whose position is non-ambiguous. The very close agreement between experimental and computed values with only two adjustable crystallographic parameters is a strong argument in favor of a unique crystalline structure in the quiescent state. The corresponding tetragonal parameters are given in Table 2 and is to notice that

* Corresponding author.
E-mail address: pierre-antoine.albouy@u-psud.fr (P.-A. Albouy).

https://doi.org/10.1016/j.polymer.2022.124760

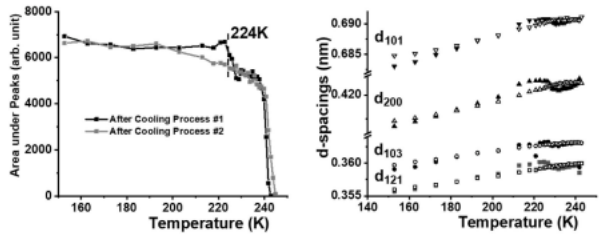

-A- -B-

Fig. 1. –A- Integral scattered intensity associated to the crystallization peaks during warming. –B- d-spacings for the first four more intense diffraction lines during warming (filled symbols: after cooling process #1; open symbols: after cooling process#2).

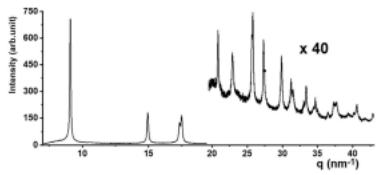

Fig. 2. Powder diffraction patterns for a vinyl-terminated linear PDMS oil measured at 223K (X-ray wavelength: 0.1542 nm).

Table 1
Comparison between observed and calculated d-spacings.

(h,k,l)-indices	Experimental d_{hkl} 234K (nm)	Calculated d_{hkl} 234K (nm)	Experimental d_{hkl} 164 K (nm)	Calculated d_{hkl} 164K (nm)
101	0.6909	0.6898	0.6867	0.6864
200	0.4207	0.4207	0.4182	0.4182
103	0.3647	0.3657	0.3605	0.3611
121	0.3591	0.3591	0.3572	0.3572
004	0.3013	0.3013	0.3003	0.3003
123	0.2746	0.2746	0.2733	0.2733
031	0.2730	0.2731	0.2716	0.2716
132	0.2450	0.2450	0.2438	0.2439
024	0.2434	0.2435	0.2425	0.2407
400	0.2103	0.2103	0.2094	0.2091

Table 2
Crystallographic parameters for the tetragonal unit cell.

Temperature	a (nm)	c (nm)	c/a
234K	0.8414	1.2050	1.432
164K	0.8366	1.2009	1.435

the ratio c/a is quite similar for both temperatures and remains very close to $\sqrt{2}$; this fact explains the high number of observed doublets. Only *hkl* reflections with the selection rule $h + k + l = 2n$ are observed that indicates body-centering condition as previously proposed [8].

Assuming the $I4_1$ assignment to be correct, the atomic coordinates of a single monomer unit are sufficient to describe the structural organization: symmetry elements generate two chains with four-fold helical conformation linked by the centering condition and running along the $\vec{c}$-axis. As mentioned in introduction no solution could be found that led to a satisfying agreement between computed and experimental line intensities [8,14]. One possible explanation to this fundamental issue is an error in the choice of the space group. A tetragonal space group with more symmetry elements is for instance possible but requires some substitutional disorder to maintain a realistic crystal density [14]. Micro-twinning between $I4_1$ and $I4_3$ crystallites can be also considered. A second disturbing fact is that the ratio c/a appears rather unchanged with temperature while the thermal expansion of the in-chain parameter c is normally expected significantly smaller than for the lateral-packing parameter a. An evaluation of the crystallographic parameters based on the four peak positions obtained during continuous warming (Fig. 1-B) confirms quite similar temperature dependences (see Fig. 3).

3.2. Crystalline texture

3.2.1. Lower draw ratio regime

In agreement with Tosaka et al. findings, no qualitative evolution of the fiber patterns is observed for elongations lower than ca.2 that corresponds to the lower draw ratio regime they assigned to the so-called "β-phase" [9]. A representative example is given in Fig. 4 where the

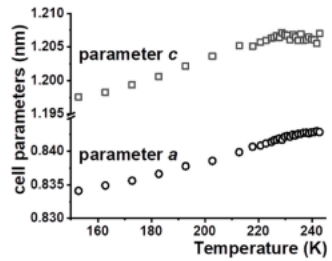

Fig. 3. Temperature dependence of the crystallographic parameters estimated from the d-spacing of the four first diffraction lines.

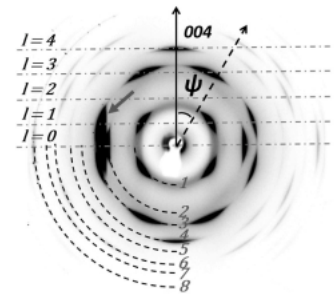

Fig. 4. Experimental fiber pattern obtained in the low draw ratio regime (150K; applied draw ratio: 1.4; effective draw ratio: 1.9); the gray arrow is pointing to some parasitic scattering.

draw axis is along the vertical. Diffraction layers are clearly identified and the corresponding hyperboles are approximated by the gray dotted lines. It illustrates the condition $l = 4$ for possible *00l* reflection mentioned in introduction and at the origin of the tetragonal assignment (4_1 screw axis) [8]. The tetragonal c-axis is parallel to the fiber axis and the tetragonal symmetry is thus compatible with the applied uniaxial symmetry.

The azimuthal location for the intensity maxima is readily computed as sketched in Fig. 5 for an assembly of crystallites that displays cylindrical symmetry and whose given [HKL] axis is assumed to perfectly align along the stretching direction. Cylindrical symmetry is assumed in accordance with the uniaxial symmetry of the applied strain. The section of reciprocal space associated to an arbitrary chosen *hkl* reflection reduces to the circle C_{hkl} that intercepts the Ewald sphere at points A and B. The corresponding diffracted beams hit the detector at points A′ and B′ and their angular deviation defines the azimuthal angle ψ_{hkl}. This angle is experimentally obtained from the angular scans underlined by the black dotted circular arcs numbered 1 to 8 in Fig. 4. Calculations presented in Table 3 have been performed assuming the above-described tetragonal unit cell with the tetragonal axis along the stretching direction: [HKL] ≡ [001]. The agreement between experimental and computed azimuthal angles is quite satisfying as previously reported by Albouy [8]. Indeed, it is necessary to introduce some fluctuation for the

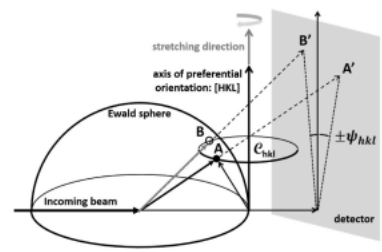

Fig. 5. Schematic representation of the diffraction geometry for a perfectly aligned fiber.

Table 3
Comparison between the calculated and experimental azimuthal locations of the fibber pattern intensity reinforcements: lower draw ratio regime.

(h,k,l)-indices	Circle number	ψ: calculated	ψ: experimental
101	1	55.0°	55.3°
200	2	90°	89.7°
103	3	24.9°	23.8°
121	3	72.6°	73.0°
004*	4	0°	0.3°
123	5	46.4°	46.1°
031	5	76.8°	80.1°
132	6	65.9°	66.7°
024	6	34.8°	33.3°
033	7	54.6°	55.1°
231	7	78.9°	78.0°
400	8	90°	89.7°

orientation of the c-axis with respect to the stretching direction so that reflections very close to or in meridional position become visible.

3.2.2. Intermediate and higher draw ratio regimes

When the draw ratio starts to exceed ca. 2, the angular distribution of intensities changes as reported by Tosaka et al. [9]. This is clearly seen in Fig. 6-A where the new location for the 004 reflection is indicated as an illustration. Some reflections that were superimposed to stronger ones or that were very weak are now well visible: an example is given by the line indexed as 112. This similarly holds for 1̄10 reflection (black arrow in Fig. 6-A, B) that cannot be detected in the quiescent state. It is insisted that all these now visible reflections are at the expected d-spacing and allowed by the $I4_1$ space group. According to Tosaka et al., no more significant evolution in the fiber pattern is observed for draw-ratios exceeding 3.5–4 [9]: this is the higher draw ratio regime they assigned to the so-called "α-phase". A representative example is given in Fig. 6-B.

As stated above we let aside the hypothesis of polymorphism and we assume that a unique crystalline structure is present while only the axis of preferential orientation has changed. In fact any deviation of the axis of preferential orientation from the tetragonal axis results in the breakage of the tetragonal symmetry. However, the radial scans obtained for low, intermediate and high draw ratios and displayed in Fig. 7 are quite similar in terms of both line locations and intensities as previously noticed by Tosaka et al. [9]. It implies that the structural modifications induced by the applied strain should remain limited, and the tetragonal crystalline structure is thus assumed unaffected in first approximation.

The question now arises of which changes in preferential orientation direction could account for the observed evolution of the fiber patterns. For this purpose, a homemade software was used to generate pattern simulations; the preferential orientation is accounted for by a Gaussian orientation function and more computational details can be found elsewhere [20]. The average direction of preferential orientation is defined by the spherical angles given in Fig. 8-A, and a systematic mapping for the diffraction patterns is performed. There again, cylindrical symmetry with respect to the direction of preferential orientation is assumed. Among the different patterns displayed in Fig. 9, those corresponding to $\varphi = 45°$ are closer to the experimental diagrams. It implies that the direction of preferential orientation remains located in the (110) plane, see Fig. 8-B. This finding can be rationalized as follows: the {100} and {010} directions are equivalent in the tetragonal symmetry which is preserved in the regime of low draw ratios. Entering the intermediate regime, this equivalence is maintained if the axis of preferential orientation remains located in the (110) diagonal plane.

It is now shown that the present hypothesis of a direction of preferential orientation located in the (110) plane is able to account quantitatively for the angular location of the intensity maxima of the patterns displayed in Fig. 6-A and B. Actually, a rapidly growing complexity of the diagrams arises from the fact that the different reflections of a given

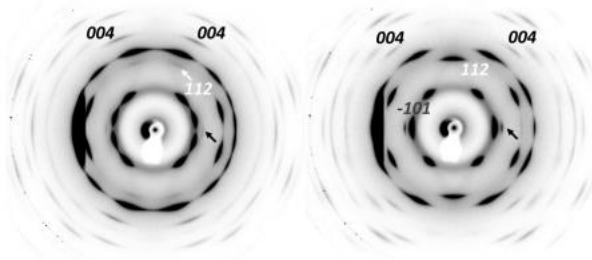

-A- -B-

Fig. 6. Representative fiber patterns for the intermediate (A) and higher (B) draw ratio regimes (150K; applied draw ratio: resp. 1.8 and 2.5; effective draw ratio: resp. 2.5 and 3.9). The black arrow points to the *1–10* reflection.

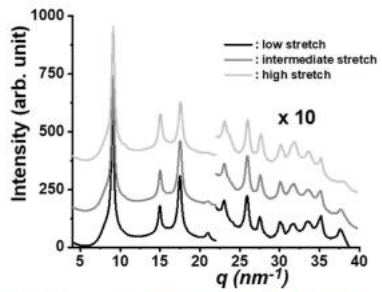

Fig. 7. Radial scans of fiber patterns displayed in Fig. 4 and 6-A,B for low, intermediate and high draw ratios.

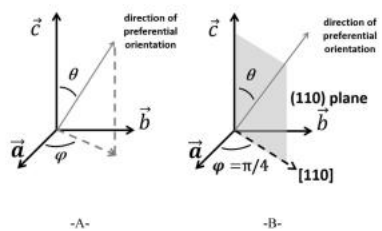

-A- -B-

Fig. 8. A: definition of the spherical angles used to characterize the direction of preferential orientation. B: actual location of the axis of preferential orientation.

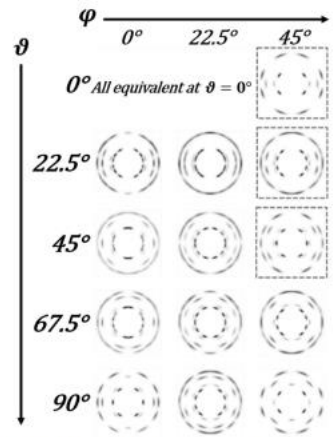

Fig. 9. Simulated fiber patterns for q-values up to 0.2 nm^{-1} for different directions of preferential orientation (spherical angles as defined in Fig. 9-A). Diffraction lines are given arbitrary intensity for illustration purpose. The full-width at half maximum of the Gaussian orientation function is fixed to 10°. For $\vartheta = 0°$ patterns are similar independent of φ.

{hkl} family now separate depending upon the sign of the h, k-indices. For the sake of simplicity only maxima associated to the first diffraction lines are thus reported. We see in Tables 4 and 5 that a nice agreement between computed and experimental azimuthal ψ_{hkl} angles is reached for directions of preferential orientation tilted respectively by $\vartheta = 25°$ and 38° with respect to the $\vec{c}$-axis.

The question now arises to know if the tilt angle ϑ may reach values higher than 38° for higher draw ratios. It is known that sol-gel filled PDMS rubbers present a rather low elongation at break [15–17] and our samples could not be extended to an elongation above 2.5, corresponding to an effective draw ratio ca. 3.9. Tosaka et al. were able to reach significantly higher draw ratios with silica powder filled samples: Fig. 10-A is reproduced from the publication [9]; the term "Latitude" used in ordinate refers to the complementary angles for the angular maxima ψ_{101} and ψ_{-101} associated to the first most intense diffraction line. Latitudes calculated with our model are plotted as a function of the tilt angle ϑ in Fig. 10-B. It readily shows that experimental angular latitudes reached at the higher strain ratios correspond to a tilt angle $\vartheta \approx 45°$, very close to the angle between the c-axis and the [111] direction (44.6°, always keeping the tetragonal unit cell as reference). The long diagonal of the unit cell represents thus the ultimate direction of preferential orientation at higher draw ratios in the frame of the texture model.

Table 4
Comparison between the calculated and experimental azimuthal locations of the fibber pattern intensity reinforcement in the intermediate draw ratio regime; tilt angle $\vartheta = 25°$.

(h,k,l)-indices	Circle number	ψ: calculated	ψ: experimental
101	1	40.1°	40.1°
−101	1	74.1°	74.4°
200	2	72.5°	72.7°
112	2	19.8°	16.7°
103	3	18°	17.1°
−103[a]	3	46.2°	46.9°
121[a]	3	49°	46.9°
−121	3	66.5°	66.6°
-1–21	3	83.5°	83.3°
004	4	24.1°	23°

[a] Positions cannot be distinguished.

Table 5
Comparison between the calculated and experimental azimuthal locations of the fiber pattern intensity reinforcement: higher draw ratio; tilt angle $\vartheta = 38°$.

(h,k,l)-indices	Circle number	ψ: calculated	ψ: experimental
101	1	35.8°	35.8°
−101	1	85.4°	85.6°
200	2	63.5°	63.3°
112	2	4.2°	0°
103	3	26.1°	26.1°
121	3	36.4°	36.8°
−121[a]	3	64.9°	66.4°
-1-21[a]	3	70.2°	66.4°
1–21	3	87.6°	90°
004	4	38.5°	38.5°

[a] Positions cannot be distinguished.

3.3. Discussion

The above-detailed "texture model" presents two attractive features. First it is possible to account precisely for the d-spacing of all diffraction lines as well in the quiescent state as under stretching with only one crystalline phase. Second it allows a quantitative and simple description of the evolution of the fiber patterns with strain. If the polymer chains are assumed to run parallel to the tetragonal axis in crystallites, the reported changes in direction of preferential orientation imply a progressive shift of the chain axis for polymers embedded into crystallites from parallel to the stretching direction at low draw ratios to tilted by ca. 45° at high draw ratio. It is to notice that Tosaka et al. similarly proposed a tilted orientation of polymer chains at higher strains for one of the crystal forms in the frame of the polymorphic model [10]. A FT-NIR spectroscopic study by Klimov et al. on the strain-induced orientation of polymer chains in silica-filled PDMS samples confirms the existence of a specific issue about this point [21]. In that case the samples were subjected to continuous mechanical cycling at room temperature, −20 °C and −40 °C. They report a specific orientation mechanism for samples cooled at −40 °C that they attribute to changes in the orientation of crystalline lamellae. More precisely the long axis of lamellae is first assumed to orient parallel to the stretching direction; lamellae break into small fibrillar fragments at higher draw ratio and reorient. Care must be taken that the present experiments are static and not dynamic, but changes in the orientation of crystalline lamellae are a possible explanation for the presently reported texture changes. Potentially linked to this question is the surprising fact that the thermal contraction is apparently similar parallel and perpendicular to the tetragonal axis. This suggests some equivalence between the [110] and [001] directions, reinforced by the fact that $\left|\vec{a} + \vec{b}\right| \approx c$. It is to notice that the direction of preferential orientation at higher strain, [111], is actually half-way both directions. The question of the chain orientation can also be raised at the light of another observation made by Tosaka et al.: they report the apparition of a well-defined intensity reinforcement in equatorial position at room temperature for draw ratios higher than ca. 2.8 [9]. It is localized slightly out of the center of the amorphous ring and some weaker and broader diffusion becomes also visible in meridional position. These authors unambiguously demonstrated this so-called "mesomorphic phase" to be different from the 3D long-range ordered crystalline phase. However, both phases must be structurally related in some way as the most intense equatorial reflection for the crystalline phase in the high-strain regime (indexed as *-101* in Fig. 6-B) and the equatorial spot for the "mesomorphic" phase are similarly located [9]. If the "mesomorphic" phase is assumed to consist in domains of well-packed parallel chains, this structural relation between both phases could imply that these bundles are oriented at 45° from the stretching axis that appears counter-intuitive.

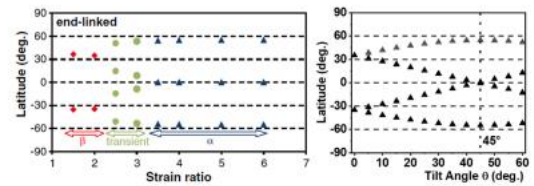

-A- -B-

Fig. 10. -A- Values for the latitude angles $90\text{-}\psi_{101}$ and $90\text{-}\psi_{-101}$ as a function of the applied strain ratio according to Ref. [8] -B- Computed latitude angles as a function of the tilt angle ϑ of the axis of preferential orientation with respect to the [001] direction.

4. Conclusion

We demonstrate in the present work that the hypothesis of changes in the crystalline texture of PDMS rubbers at low temperature explains in a quantitative manner the evolution of the fiber patterns, without needing to introduce additional crystal phases. The actual crystalline structure should remain very close to the initial tetragonal organization, whatever this last is. The axis of preferential orientation is the tetragonal axis at lower strain and it progressively shifts towards the [111] long diagonal at higher strain while remaining into the (110) plane at intermediate strain.

This description is an alternative to the polymorphism proposed by Tosaka et al. and further investigations are needed to discriminate between both models. The fundamental remaining issue is a working structural model and linked to this is the assessment of the orientation of the polymer chains embedded into the crystalline phase for different draw ratios. The FT-NIR technique mentioned above could bring an answer [21].

CRediT authorship contribution statement

Xiang Shi: Investigation and funding acquisition. **Pierre-Antoine Albouy:** Supervision and writing. **Pascale Launois:** Software.

Declaration of competing interest

The authors declare that they have no known competing financial interests or personal relationships that could have appeared to influence the work reported in this paper.

Acknowledgement

We thank Stéphan Rouzière (head of the X-ray platform "MORPHEUS" at the Laboratory) for his precious help. One of us (Xiang Shi) would like to also thank the Chinese Scholarship Council for its financial help. Pascale Launois thanks Geoffrey Monet for the initial development of the simulation program presently used.

References

[1] P. A Klonos, Crystallization, glass transition and molecular dynamics in PDMS of low molecular weights: a calorimetric and dielectric study, Polymer 159 (2018) 169–180.

[2] A. Maus, K. SaalwÃchter, Crystallization kinetics of poly(dimethylsiloxane) molecular-weight blends – correlation with local chain order in the melt, Macromol. Chem. Phys. 208 (2007) 2066–2075.

[3] T. Dollase, H. W Spiess, M.Gottlieband R. Yerushalmi-Rozen, Crystallization of PDMS: the effect of physical and chemical crosslinks, Europhys. Lett. 60 (2002) 390–396.

[4] M. I Aranguren, Crystallization of polydimethysiloxane: effect of silica filler and curing, Polymer 20 (1998) 4897–4903.

[5] C. M Roland, C.A. Aronson, Crystallization of polydimethylsiloxane end-linked networks, Polym. Bull. 45 (2000) 439–445.

[6] G. Damaschun, , Röntgenographische Untersuchung der Struktur von Silikongummi, Z. Kolloid, Z. Polym. 180 (1962) 65–67.

[7] F. C Schilling, M.A. Gomez, A. E Tonelli, Solid-state NMR observations of the crystalline conformation of poly(dimethylsiloxane), Macromolecules 24 (1991) 6552–6653.

[8] P.-A. Albouy, The conformation of poly(dimethylsiloxane) in the crystalline state, Polymer 41 (2000) 3083–3086.

[9] M. Tosaka, M. Noda, K. Ito, K. Senoo, K. Aoyama, N. Ohta, Strain- and temperature induced polymorphism of poly(dimethylsiloxane), Colloid Polym. Sci. 291 (2013) 2719–2724.

[10] M. Tosaka, K. Tashiro, Crystal polymorphism and structure models of Poly (dimethylsiloxane), Polymer 153 (2018) 507–520.

[11] J.Y. Zhao, P.Z. Chen, Y.F. Lin, J.R. Chang, A. Lu, W. Chen, L. P Meng, D. L Wang, L. B. Li, Stretch-induced crystallization and phase of poly(dimethylsiloxane): an in situ synchrotron radiation wide-angle X-ray scattering study, Macromolecules 51 (2018) 8424–8434.

[12] J.Y. Zhao, P.Z. Chen, Y.F. Lin, W. Chen, A. Lu, L. P Meng, D. L Wang, L.B. Li, Stretch-induced intermediate structures and crystallization of poly (dimethylsiloxane): the effect of filler content, Macromolecules 53 (2020) 719–730.

[13] J.Y. Zhao, S. Feng, W. W Zhang, W. Chen, J. F Sheng, W.C. Yu, L.B. Li, Strain rate dependence of stretch-induced crystallization and crystal transition of poly (dimethylsiloxane), Macromolecules 54 (19) (2021) 9204–9216.

[14] **X. Shi, The Crystalline Structure of Polydimethylsiloxane: Additional Results and Additional Questions, PhD Thesis, 2021. Université Paris-Saclay, France (**https://tel.archives-ouvertes.fr/tel-03266623/document.

[15] J. M Breiner, J.E. Mark, Preparation, structure, growth mechanisms and properties of siloxane composites containing silica, titania or mixed silica-titania phases, Polymer 39 (1998) 5483–5493.

[16] L. Dewimille, B. Bresson, L. Bokobza, Synthesis, Structure and morphology of poly (dimethylsiloxane) networks filled with *in situ* generated silica particles, Polymer 46 (2005) 4135–4143.

[17] Y.-L. Yue, C. Zhang, H. Zhang, D.-H. Zhang, X. Chen, Y.-F. Chen, Z. Zhang, Tensile properties of *in-situ* precipitated polydimethyl siloxane networks, Express Polym. Lett. 7 (2013) 863–872.

[18] M. Soutzidou, A. Panas, K. Viras, Differential scanning calorimetry (DSC) and Raman spectroscopy study of poly(dimethylsiloxane), J. Polym. Sci. B Polym. Phys. 36 (1998) 2805–2810.

[19] J. I Langford, A.J. C Wilson, Scherrer after sixty years: a survey and some new results in the determination of crystallite size, J. Appl. Crystallogr. 11 (1978) 102–113.

[20] **[G. Monet; PhD thesis, The Python Program Was Initially Developed by G. Monet to Compute in an Optimized Way the Diffraction of Perfectly Oriented Tubular Objects in Three Dimensions, 2019,** https://tel.archives-ouvertes.fr/tel-02389285. **It was further implemented by P. Launois and G. Monet to calculate diffraction of tubular objects organized in fibers, with given disorientation with respect to the fiber axis, and to simulate the data recorded on a two-dimensional detector.**

[21] E. Klimov, G.G. Hoffmann, A. Gumenny, H. W Siesler, Low-temperature FT-NIR spectroscopy of strain-induced orientation and crystallization in a poly (dimethylsiloxane) network, Macromol. Rapid Commun. 26 (2005) 193–1098.